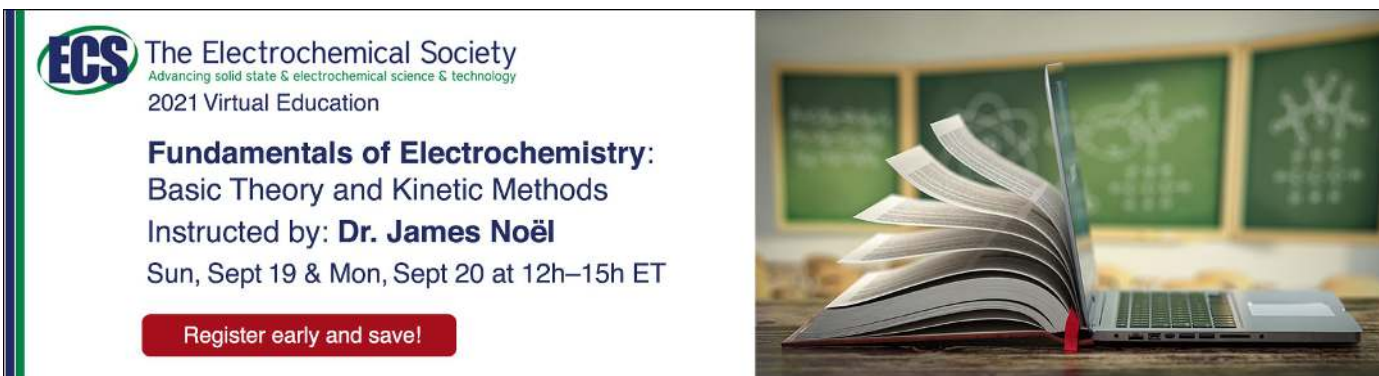**PAPER • OPEN ACCESS**

Investigation of thermal properties of Al1050/SS304 sandwich composite sheet by using a numerical, analytical and experimental approach

View the article online for updates and enhancements.

Materials Research Express

PAPER

Investigation of thermal properties of Al1050/SS304 sandwich composite sheet by using a numerical, analytical and experimental approach

Atul S Takalkar [ORCID] and Lenin Babu Mailan Chinnapandi [ORCID]

School of Mechanical and Building Sciences, Vellore Institute of Technology, Chennai, Tamil Nadu, India

E-mail: lenin.babu@vit.ac.in

Abstract

The utilization of the sandwich composite sheets for the specific industrial application depends upon its material properties. The present study investigates the mechanical and thermal properties of Al1050/SS304 sandwich composite sheets which could be used for the manufacturing of automobile sheet metal components such as a car body. The XRD (X-ray powder diffraction) and FTIR (Fourier-transform infrared spectroscopy) are performed to investigate the molecular structural arrangement and adhesive bonds whereas the composite wall test is performed to investigate the thermal conductivity by using different approaches. The experimental approach integrated with the analytical approach is utilized to validate the obtained thermal conductivity using a numerical approach. The thermal conductivity of 2.84 W mK^{-1} is obtained by using a numerical approach which is in good correlation with the experimental results.

1. Introduction

The thermal energy is observed to be transferred due to the temperature difference between the two surfaces. The rate of transfer of thermal energy depends on the material properties such as thermal conductivity and further may vary due to material non-homogeneity. This material non-homogeneity plays a significant role in the thermal conductivity of the composite materials.

Recently, a lot of researchers had investigated the thermal conductivity of the different composite materials by using different approaches. Piedra *et al* [1] carried out the thermal analysis of the primary composite structure of a CubeSat manufactured by using carbon fibre/epoxy resin composite materials with Zinc oxide nanoparticles. The simulation was performed in three different orbit inclusion angles where the radiative heat fluxes were applied over composite panels in orbit trajectory. The rise in temperature gradients between the panels and the reduction in heat transfer in the structure of Cubesat was observed due to lower thermal conductivity.

Joshi *et al* [2] studied the temperature distribution and heat transfer through Glass/BMI honeycomb core aerogel-filled sandwich panels using numerical and experimental approaches. The temperature bearing capacity and operating temperature were increased by changing the coating process. The temperature sustainability was found to be increased to 350 °C for silicone-based coating. Whereas Vitale *et al* [3] studied the density and the thermal properties of the honeycomb sandwich panels. The vacuum infusion technique was utilized to bond the jute fibre composite skin and glass to different cores like honeycombs, wood, and Diviny cell. It was observed that the sandwich panels manufactured with carbon fibre honeycomb do not meet the requirement of the thermal insulator of thermal conductivity of 0.15 W mK^{-1}. Similarly, the thermal and mechanical performance of pyramidal core sandwich panels used in aircraft was also investigated by Zhang *et al* [4] by carrying out 2D thermal transfer analysis.

Few of the researchers had focused on the calculation of the thermal conductivity of nanocomposite materials. Zhu *et al* [5] investigated the effect of copper nanoparticles and copper nanowires on thermal

Table 1. Material properties of the sheets used for experiments.

Properties	Bakelite [13]	Steel [13]
Thermal conductivity (W mK^{-1})	0.97	41.31

conductivity of dimethicone nanocomposite material using a theoretical and experimental approach. The obtained thermal conductivity of dimethicone nanocomposite material by addition of 10% volume of copper nanoparticles was 0.25 W mK^{-1} whereas the improved thermal conductivity of 0.41 W mK^{-1} was observed by the addition of 10% volume of copper nanowires. Similarly, the high thermal conductivity was observed by Li *et al* [6] for nickel-epoxy nanocomposites. It was found that the particle size of 40 nm shows the thermal conductivity of 0.37 W mK^{-1} whereas the thermal conductivity of the particle size of 70 nm was 0.31 W mK^{-1}.

Apart from fibre/epoxy resin composite and carbon fibre honeycomb, the utilization of Aluminium metal in the composite sheet was observed to be favoured by a lot of researchers due to high thermal conductivity and lightweight. Quintana *et al* [7] studied the thermal conductivity and plate bending behaviour of sandwich panels manufactured by using graphitic-foam cores, Aluminium face sheets, and carbon-fibre face sheets. The experimentally obtained results were validated by using an analytical model where it was observed that the tendency of unwanted thermal distribution was able to reduce with the use of graphitic foam as core material. Similarly, Kulhavy *et al* [8] studied the thermodynamic behaviour of two different heat hexagonal structure shield manufactured by using an Aluminium plate and composite plate (manufactured by using lamination and diffusion of the glass fabric process). The numerical and experimental approaches were utilized to determine the heat transfer efficiency between the sheet surface and surrounding airflow. The thermal field distribution was observed to be homogeneous for the composite material as compared to the Aluminium. The thermal analysis of the doubly curved sandwich panel manufactured by using Aluminium skin, polyethylene core, and epoxy resin was also carried out by Patel *et al* [9]. The numerical simulation was carried out by considering the one-dimensional heat flow model to investigate the thermal infiltration of heat flux through composite material. The 47.73% high thermal infiltration was observed for Aluminium material compared to sandwich material.

Similar to Aluminium, few researchers had utilized the Steel metal skin in the sandwich composite sheets due to moderate thermal conductivity and high formability. Yang *et al* [10] investigated the thermal conductivity of steel/polyester composite material by using a numerical approach. The thermal conductivity of 0.87 W mK^{-1} was observed for the composite material. The thermal transmission was found to be increased with an increase in steel wire in the longitudinal direction but observed to be decreased in the transverse direction. Also, the thermal conductivity of the metal/polyester composite solid model was observed to be increased to 0.68 W mK^{-1} due to the utilization of steel wires [11].

From the literature, it is observed that the thermal conductivity of the metal/polymer sandwich composite sheet can be improved by the utilization of the combination of the sandwiched materials, different manufacturing techniques, and processes. The review [12] explores that such composite sheets along with the different techniques like hydro-mechanical and reverse deep drawing at the elevated temperature can help to achieve the higher LDR and lower thickness variation in the deep drawing process.

The Al1050/SS304 sandwich composite sheet is deep drawn to complex profiles and can be utilized for the manufacturing of automobile components such as car body and cabin where the heating problem is frequently observed. The investigation of the thermal properties of such materials used in car bodies needs to be carried out to increase the effectiveness of the component. In the present study, the analytical approach integrated with the experimental approach has been utilized for the accounting of thermal conductivity of the Al1050/SS304 sandwich composite sheets. Along with these approaches the numerical approach has also been utilized for the investigation of the thermal conductivity of the sandwich composite materials.

2. Materials

The experimental setup consists of a sequential combination of the different materials such as Bakelite and Steel of the diameter of 100 mm. The thermal properties of these materials are shown in table 1. The manufactured sample of Al1050/SS304 sandwich composite material with a diameter of 100 mm is inserted between these standard referred materials.

In the case of manufactured sandwich composite metal sheet, the Al1050 sheet contributes to the reduction of weight whereas the SS304 sheet contributes to increasing the formability. These two properties are required for the manufacturing of the automobile components effectively. The selected material sheets of Al1050 and SS304 for the manufacturing of the sandwich composite are bound together by using Urethane methacrylate ester structural adhesive. The material properties of the sandwich sheets and binder are shown in table 2.
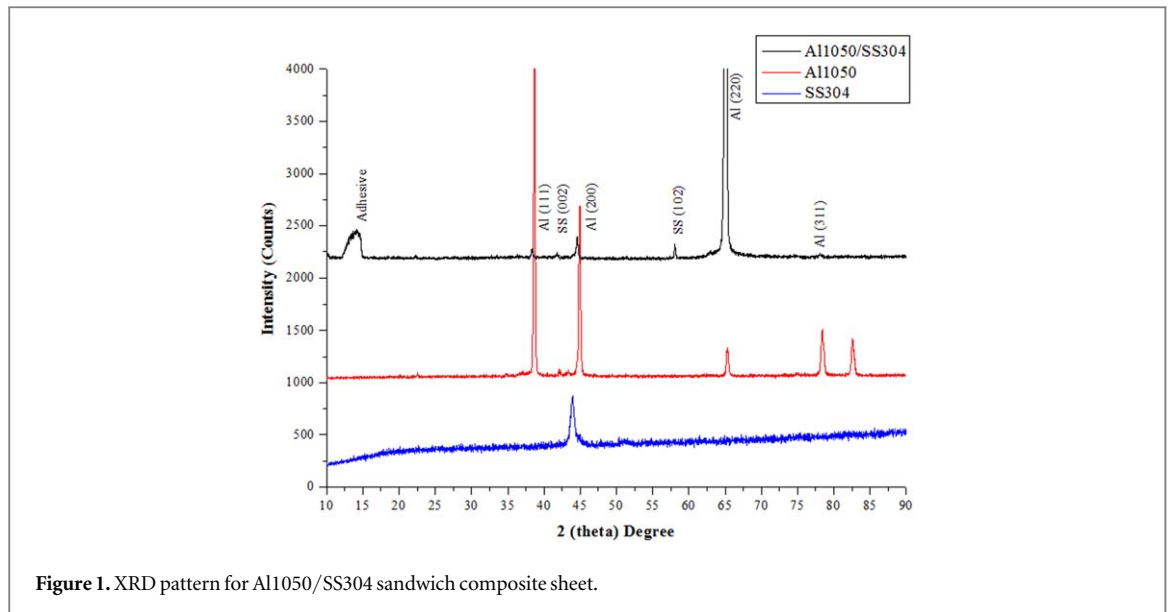
Figure 1. XRD pattern for Al1050/SS304 sandwich composite sheet.

Table 2. Material properties of sandwich composite sheets.

Properties	Al1050 [14]	Adhesive [15, 16]	SS304 [17]
Density (kg m^{-3})	2710	1235	8000
Young's modulus (GPa)	70	1.4	193
Tensile strength (MPa)	178	34	476
Poisson's ratio	0.33	0.3	0.3
Thermal conductivity (W/mK)	227	0.25	16.2

Further, the study of molecular structural arrangement and adhesive bonds bonding properties is accounted for performing different tests such as XRD and FTIR.

2.1. XRD

The XRD test is performed to characterize the orientation of molecules in Al1050/SS304 sandwich composite material. The XRD pattern of the Al1050/SS304 sample is analyzed within the range of 10° to 90° with a step size of 0.02° and scan step time of 1 s. The sample of 10 mm ×10 mm is prepared for the XRD test where Cu is used as an anode material having a wavelength of 1.54059 Å. The obtained XRD pattern of the Al1050/SS304 sample is analyzed by using a JCPDS card [00–001–1179 and 00–018–0388] index file. In the present study, the analysis of the diffraction pattern is carried out to calculate the crystal size, texture coefficient, and strain. The tested specimens exhibit similar patterns that reveal the presence of Aluminium and Stainless steel metal. The sharp diffraction peaks correspond to the crystalline nature of Al1050 and SS304 layer [18–24] whereas diffused diffraction peaks correspond to the amorphous nature of the Adhesive layer [25]. The XRD test shows a sharp peak at an angle of 38.3522°, 44.5826°, 65.1824°, 78.1247° which corresponds to Al1050 and 42.8806°, 58.0493° angles corresponds to SS304 which are in good correlation with the literature and standard database. The obtained sets of distinct textures for respective angles in case of Al1050 metal are {111}, {200}, {220}, {311} and {002}, {102} for SS304 as shown in figure 1.

The structural adhesive used to clad both the metals are in an amorphous state which represents broad peaks between 10° to 15°. The XRD results show a higher intensity (counts) of 9293 for {220} plane at 64° in the case of the Al1050 layer whereas in the case of the SS304 layer the higher intensity (counts) of 244 is observed for {102} planes at 58°. The crystallite size is calculated by using equation (1) [26],

$$D = \frac{0.9\lambda}{\beta \cos \theta} \tag{1}$$

where, D is the crystallite size and λ is the x-ray wavelength. The θ represents the Bragg's angle whereas the β is the full-width of the diffraction line at the half of its Full Width Half Maximum (FWHM). The obtained crystallite size for the Al1050/SS304 sandwich composite sheet is 369.997 Å. The orientation of the Al1050/SS304 sandwich composite sheet is studied by calculating the texture coefficient TC(hkl) of (hkl) plane using equation (2) [26],

$$TC_{(hkl)} = \frac{\dfrac{l(hkl)}{l_0(hkl)}}{\dfrac{1}{N}\sum \dfrac{l_{(hkl)}}{l_{0(hkl)}}} \tag{2}$$

where, $l(hkl)$ is the measured intensity of peak and l_0 is the standard intensity of (hkl) plane from JCPDS card [00–001–1179 and 00–018–0388]. The N is the number of reflections observed. The obtained texture coefficient TC(hkl) for the Al1050 sheet and SS304 sheet is 3.81(220) and 1.91 (102) [19–25]. The strain (ε) in the Al1050 and SS304 sheet utilised for the manufacturing of the Al1050/SS304 sandwich composite is determined by using equation (3) [26].

$$\beta = \frac{\lambda}{D\cos\theta} - \varepsilon\tan\theta \tag{3}$$

where, β is the FWHM and λ is the wavelength of x-ray. The D represents the calculated crystallite size whereas θ is the Bragg's angle. By taking the slope of the graph of $(\beta\cos\theta)/\lambda$ versus $\sin\theta/\lambda$ the average strain is calculated. The strain of 0.00306 is obtained for the Al1050 sheet whereas the strain of 0.03153 is obtained for the SS304 sheet.

2.2. FTIR

The FTIR is conducted to study the internal bonding properties of the structural adhesive material used to manufacture the Al1050/SS304 sandwich composite material. The IR is plotted separately for two different cases where the case-I consists of structural adhesive layup on the Al1050 sheet and case-II consist of activator layup on the SS304 sheet. The IR spectrum for a case-I shows peaks at 2922 cm^{-2} and 2852 cm^{-2} which indicates the presence of –C–H– bond as stretching vibration of adhesive material whereas the peak at 1732 cm^{-2} confirms the presence of ester group (–COO) of adhesive material [27]. The observed peak at 1540 cm^{-2} represents the stretching vibrations of the alkene (C=C) group of adhesive material [28, 29] whereas peaks at 1223 cm^{-2} and 1160 cm^{-2} indicate the stretching frequencies of ether (C–O) linkage [27] which can be observed from figure 2(a). The IR spectrum for case-II showed peaks at 2927 cm^{-2} and 2859 cm^{-2} indicating the stretching vibrations of the C–H bond [30, 31] of activator whereas the alkene (C=C) functionality of activator [32] is observed at 1582 cm^{-2}. The peaks at 1361 cm^{-2}, 1169 cm^{-2}, and 1038 cm^{-2} correspond to the C-N group [31–33] of adhesive material which can be observed from figure 2(b).

3. Approaches

The different methods and approaches such as analytical, experimental, and numerical have been utilized for the investigation of the thermal conductivity of the Al1050/SS304 sandwich composite material. The obtained experimental temperature difference for the steady-state condition has been utilized for the calculation of thermal conductivity by using an analytical approach. Further, the numerical simulation is carried out by replicating the same condition as an experimental approach to calculate the heat flux and thermal conductivity.

3.1. Analytical approach

The energy is transferred when the thermal gradient is maintained between the two surfaces. The maintained thermal gradient due to conduction will be proportional to the rate of the amount of energy per unit area. The heat flux (Q) can be calculated by using equation (4) [3],

$$Q = -\lambda.A.\frac{\partial t}{\partial x} \tag{4}$$

where, λ is thermal conductivity, A is the contact area and $\frac{\partial t}{\partial x}$ is temperature gradient normal to the A. Similarly, the heat flux for the composite wall can be calculated by using equation (5). The schematic representation of the temperature gradient across the composite wall is shown in figure 3.

$$Q = \lambda_1.A.\frac{(T_1 - T_2)}{L_1} = \lambda_2.A.\frac{(T_2 - T_3)}{L_2} = \lambda_3.A.\frac{(T_3 - T_4)}{L_3} \tag{5}$$

Therefore, the thermal conductivity for the ith plate can be calculated by using equation (6).

$$\lambda_i = \frac{Q}{A}.\frac{L_i}{(T_i - T_{i+1})} \tag{6}$$
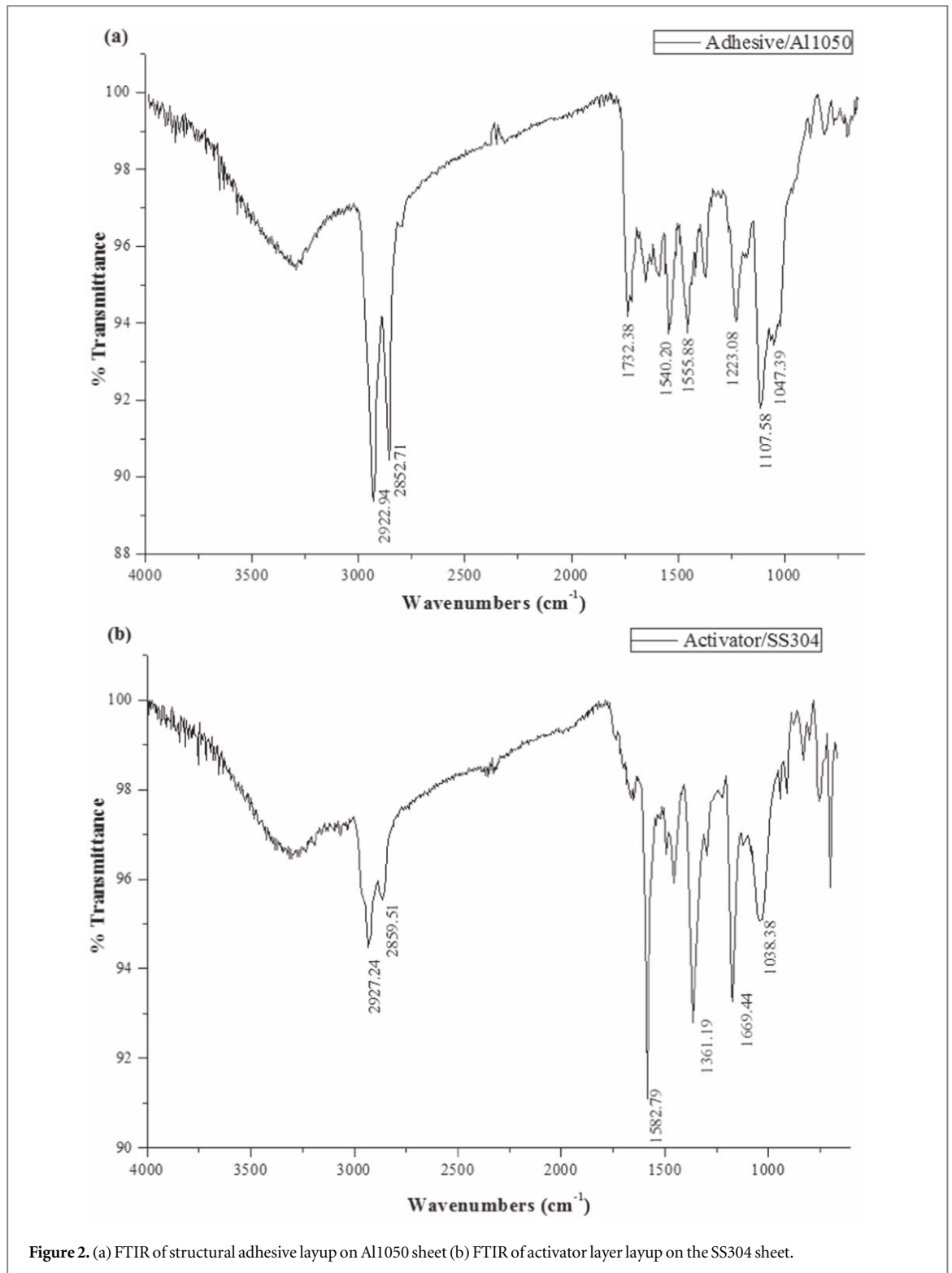
Figure 2. (a) FTIR of structural adhesive layup on Al1050 sheet (b) FTIR of activator layer layup on the SS304 sheet.

3.2. Experimental approach

The composite wall experimental setup [13, 34, 35] has been constructed for the calculation of the thermal conductivity of the Al1050/SS304 sandwich sample which consists of reference material such as Bakelite and Steel arranged in the sequence as shown in figure 4 and other units like power measurement unit, electronic voltage regulator, digital temperature indicator, heater and thermocouples as shown in figure 5. The Al1050/SS304 sandwich sample is placed between the Bakelite and Steel plate along with the thermocouples at the top and bottom of the sandwich composite sample to account for the temperature difference. This setup is further placed in the insulated cabin and clamped at both ends using a clamping fixture. The heater is used for the generation of thermal energy by setting up the defined values of the current and voltage. The generated thermal energy is allowed to pass from the Bakelite plate towards the Steel plate. T_1 and T_2 represent the temperature at
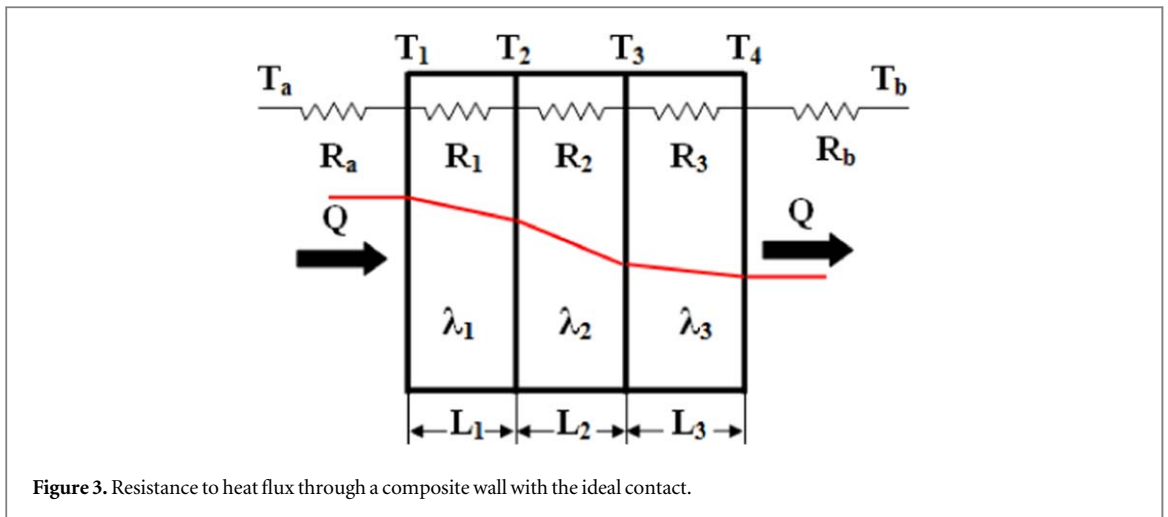
Figure 3. Resistance to heat flux through a composite wall with the ideal contact.
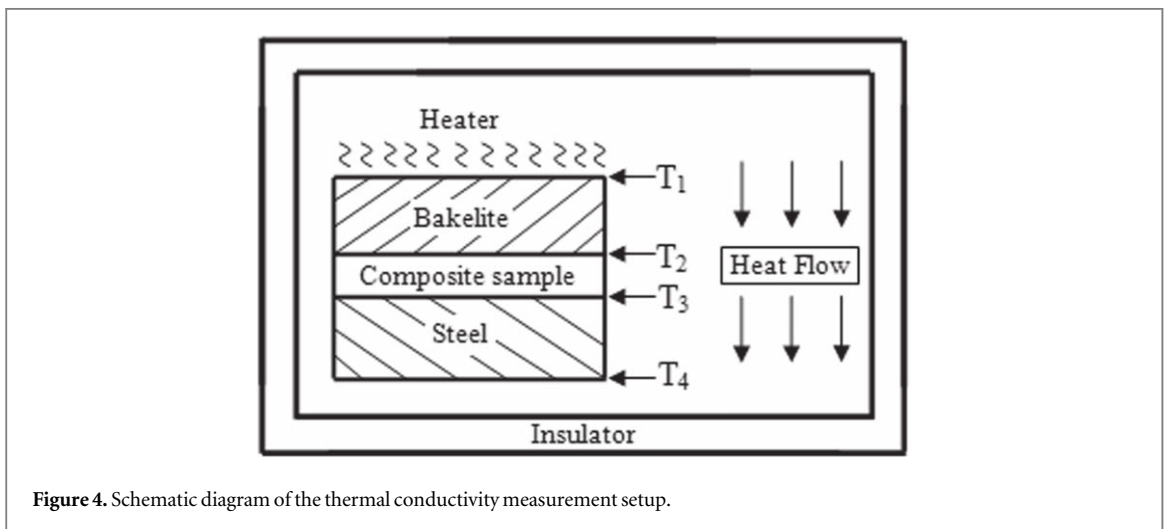

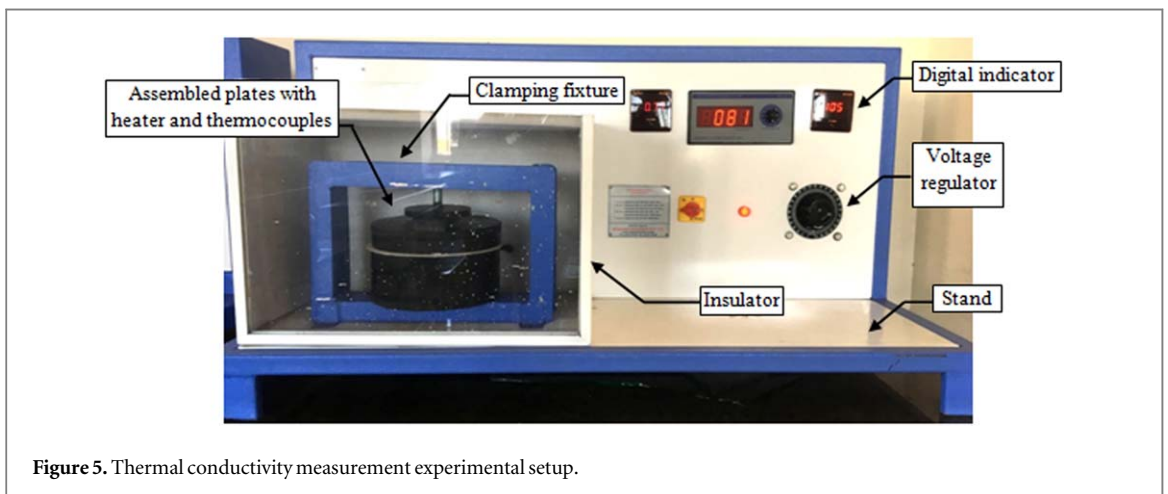**Figure 4.** Schematic diagram of the thermal conductivity measurement setup.

Figure 5. Thermal conductivity measurement experimental setup.

the upper and lower surface of the Bakelite plate whereas the T_3 and T_4 represent the temperature at the upper and lower surface of the Steel plate. As the study only focuses on the thermal characterization of the composite sample, the temperature T_2 and T_3 are considered for further calculations.

3.3. Numerical approach
The separate layers of Al1050, adhesive, and SS304 are modelled as shown in figure 6 where the k and t represent the thermal conductivity and thickness of the respective materials. The modelled layers are further discretization
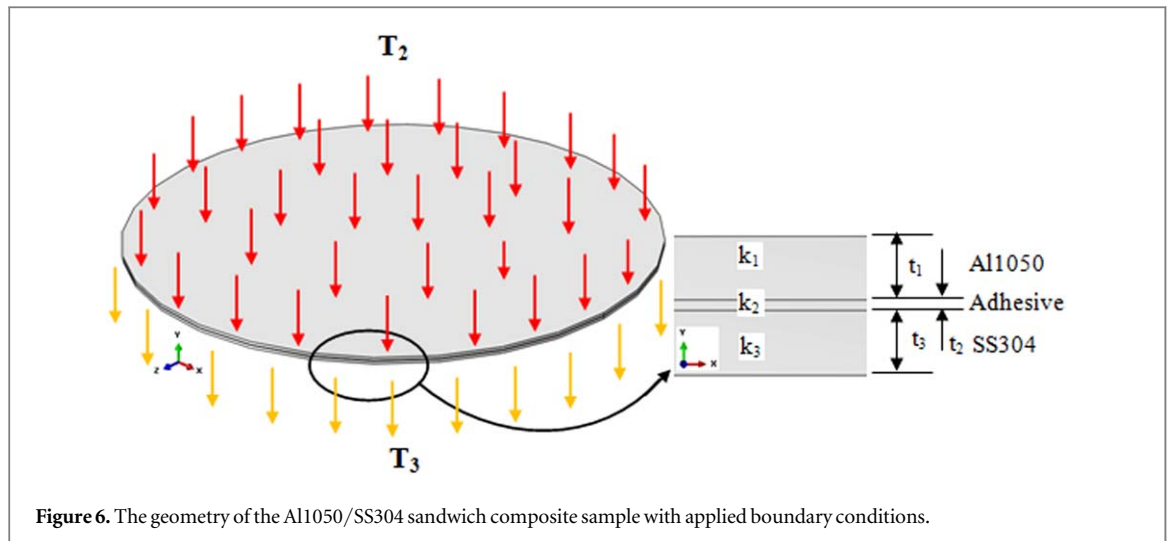
Figure 6. The geometry of the Al1050/SS304 sandwich composite sample with applied boundary conditions.
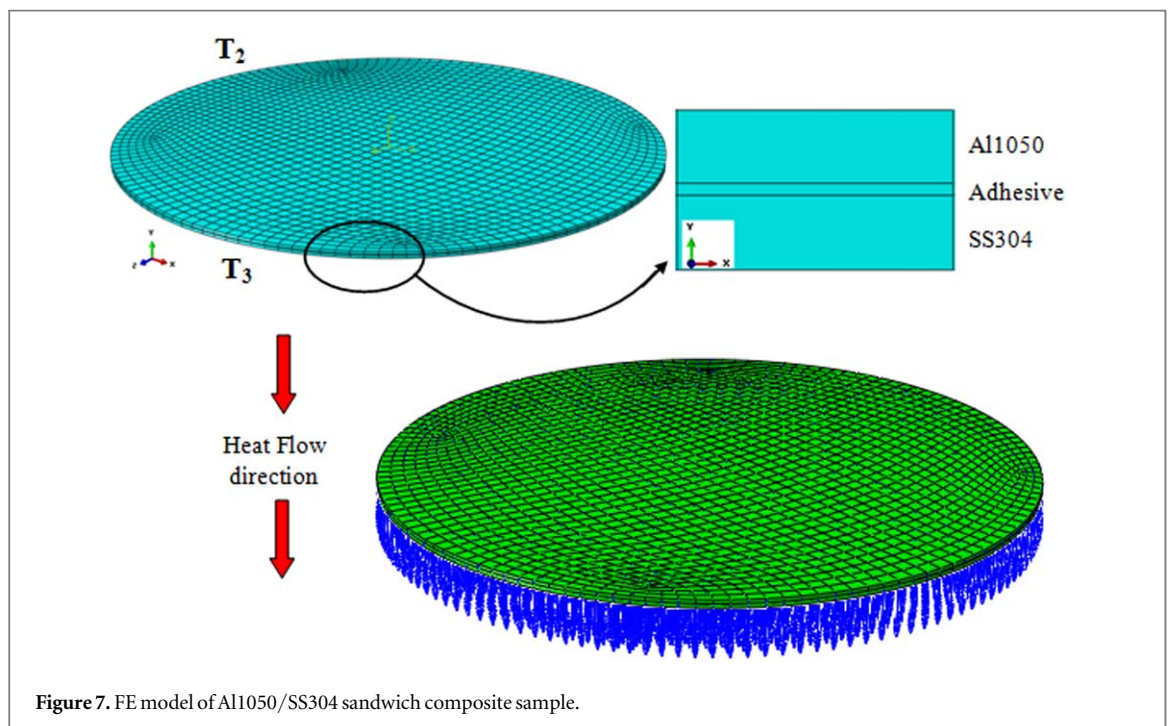

Figure 7. FE model of Al1050/SS304 sandwich composite sample.

by using hexahedron elements and assembled in the sequence as shown in figure 7 by using tie constraints. The temperature (T_2) is applied in the normal direction to the upper surface whereas the temperature (T_3) is applied at another side. The implicit heat transfer analysis is carried out by using finite element analysis ABAQUS® software by considering the steady-state response.

4. Result and discussion

The proposed experimental setup with the defined current and voltage is maintained for the specific time duration to attain the thermal equilibrium state. After achieving the thermal equilibrium state, the successive readings are recorded for every half an hour by using a digital temperature indicator. The heat flux of 53.4 Watt is defined by setting up the current and voltage. For the defined heat flux the temperature of 119 °C is observed at the upper surface (T_3) and the temperature of 116 °C at the lower surface (T_2). The obtained temperature difference and heat flux are further utilized for the calculation of the thermal conductivity (W/mK) using equation (3). The experimentally calculated thermal conductivity for Al1050/SS304 sandwich composite material is 2.93 W mK^{-1}.

The experimentally obtained thermal conductivity by maintaining the temperature boundary condition of T_2 and T_3 is also verified by performing FE simulation. The obtained temperature difference throughout the
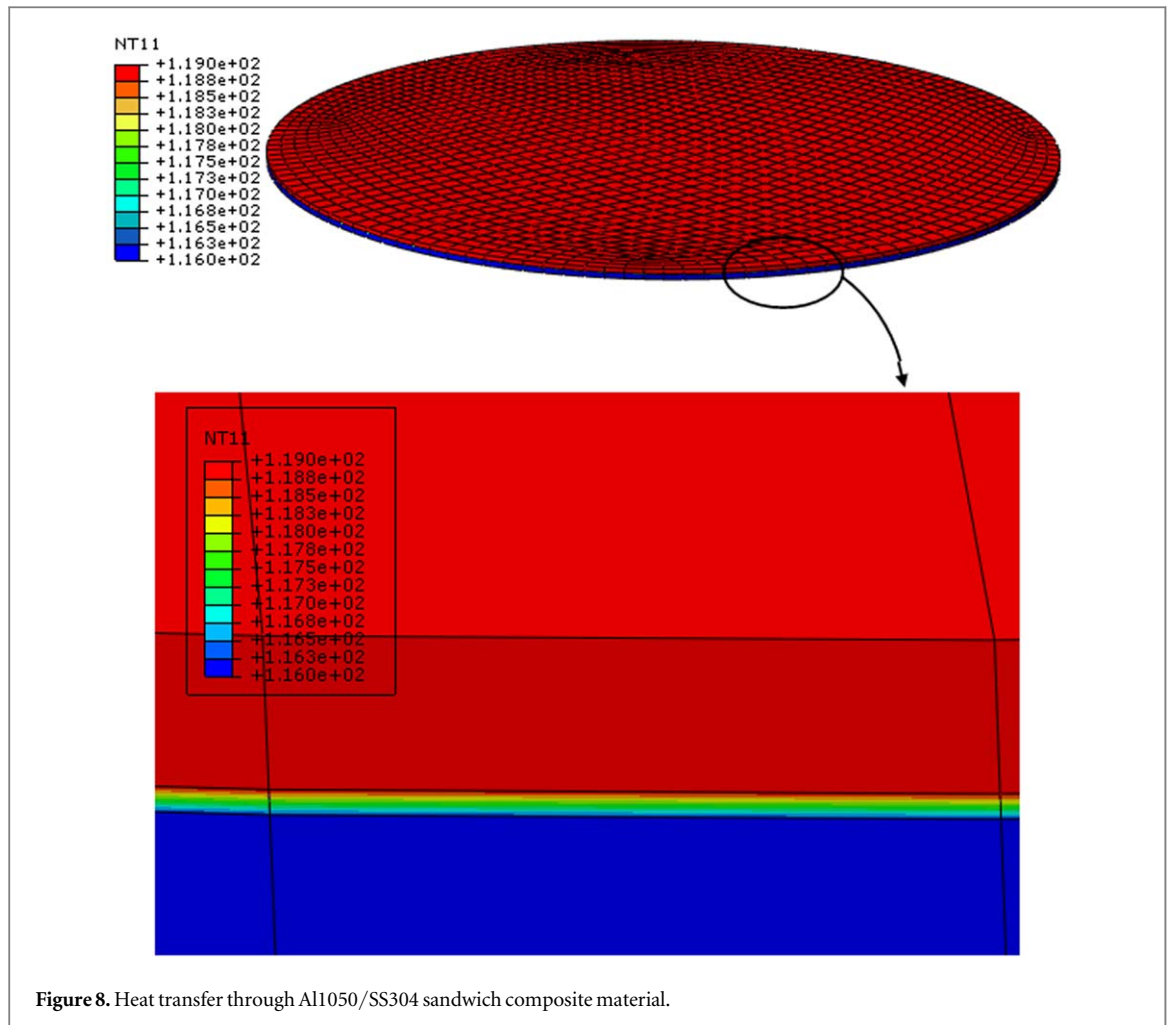
Figure 8. Heat transfer through Al1050/SS304 sandwich composite material.

sandwich composite sheet is shown in figure 8. The heat flux of 51.9 Watt is obtained for the applied temperature of 119 °C and 116 °C. The calculated thermal conductivity by using equation (3) is 2.84 W mK^{-1}.

5. Conclusions

The present study investigates the thermal properties of the Al1050/SS304 sandwich composite sheet manufactured by using a cladding process which can be utilized for deep drawing of automobile and aerospace components. The strain of 0.00306 is obtained for the Al1050 layer whereas the strain of 0.03153 is obtained for the SS304 layer. The crystallite size of 369.997 Å is obtained for the Al1050/SS304 sandwich composite.

The thermal conductivity of the Al1050/SS304 sandwich composite sheet is successfully calculated by using analytical, numerical and experimental approaches. The thermal conductivity of 2.93 W mK^{-1} is obtained by using the experimental approach whereas the thermal conductivity of 2.84 W mK^{-1} is obtained by using a numerical approach. The obtained thermal conductivity using different approaches found to have a good correlation.

Due to low thermal resistivity, the proposed lightweight Al1050/SS304 sandwich composite material can be effectively utilized for the manufacturing of the car body, roof, and doors. The utilization of the Al1050/SS304 sandwich composite material for the car body can help to maintain the inner temperature of the car passenger cabin when used in high intense sunlight.

The increase in the thickness of the adhesive layer in the Al1050/SS304 sandwich composite sheet may result in a decrease in the thermal conductivity of the sandwich composite sheet due to the low thermal conductivity of the adhesive layer. Further, the study needs to be carried out to investigate the effect of sandwich sheet thickness variation on the thermal conductivity of the Al1050/SS304 sandwich composite sheet. This can help to optimize the thickness of sandwich layers in the Al1050/SS304 sandwich composite sheet resulting in identifying the appropriate application in the field of automobiles and aerospace.

ORCID iDs

Atul S Takalkar ⬤ https://orcid.org/0000-0002-2401-3581
Lenin Babu Mailan Chinnapandi ⬤ https://orcid.org/0000-0002-4378-5149

References

[1] Piedra S, Torres M and Ledesma S 2019 Thermal numerical analysis of the primary composite structure of a CubeSat *Aerospace* **6** 97
[2] Joshi S C, Sheikh A A, Dineshkumar A and Yong Z 2016 Development and evaluation of aerogel-filled BMI sandwich panels for thermal barrier applications *AIMS Mat. Sci.* **3** 938–53
[3] Vitale J P, Francucci G and Stocchi A 2017 Thermal conductivity of sandwich panels made with synthetic and vegetable fiber vacuum infused honeycomb cores *J. Sandwich Struc. Mat.* **19** 1–17
[4] Zhang R, Zhang X, Lorenzini G and Xie G 2016 Material combinations and parametric study of thermal and mechanical performance of pyramidal core sandwich panels used for hypersonic aircrafts *Continuum Mech. Thermodyn.* **28** 1905–24
[5] Zhu D, Yu W, Du H, Chen L, Li Y and Xie H 2016 Thermal conductivity of composite materials containing copper nanowires *J. Nanomat.* **2016** 3089716
[6] Li X, Park W, Chen Y P and Ruan X 2017 Effect of particle size and aggregation on thermal conductivity of metal–polymer nanocomposite *J. Heat Trans.* **139** 022401
[7] Quintana J M and Mower T M 2017 Thermomechanical behavior of sandwich panels with graphiticfoam cores *Mat. Desig.* **135** 411–22
[8] Kulhavy P and Egert J 2017 Thermal properties of highly structured composite and aluminium sheets in an aerodynamic tunnel *EPJ Web of Conferences* **143** 02059
[9] Patel J M and Modi B A 2013 Stiffness and thermal analysis of doubly curve sandwich panel for an automobile application *Procedia Engineering* **51** 655–64 . Chemical, Civil and Mechanical Engineering Tracks of 3rd Nirma University International Conference (NUiCONE 2012)
[10] Yang F, Jin Y and Qian X 2013 Simulation of thermal conductivity of sandwich composite *Appl. Mech. Mat.* **278–280** 523–6
[11] Jin Y, Zhang C, Qian X and Yang F 2014 Effect of model structure on thermal conductivity of sandwich composites *Adv. Mat. Res.* **941–944** 2478–81
[12] Takalkar A S and Babu L M C 2019 Deep drawing process at the elevated temperature: a critical review and future research directions *CIRP J. Manuf. Sci. Tech.* **27** 56–57
[13] Mukhraiya V, Yadav R and Kori S 2016 Thermal conductivity analysis in various materials using composite wall apparatus *Inter. J. Mech. Eng. Tech.* **7** 342–50
[14] Lim S S, Kim Y T and Kang C G 2013 Fabrication of aluminum 1050 micro-channel proton exchange membrane fuel cell bipolar plate using rubber-pad-forming process *The Int. J. Adv. Manuf. Tech.* **65** 231–8
[15] Loctite® AA 324™ 2018 Technical Data Sheet. (www.henkel-adhesives.com/in/en/product/structural-adhesives/loctite_aa_324.html)
[16] Nejad S J 2012 A review on modeling of the thermal conductivity of polymeric nanocomposites *e-Polymers* **12** 025
[17] Jeong M G, Jin C K, Hwang G W and Kang C G 2014 Formability evaluation of stainless steel bipolar plate considering draft angle of die and process parameters by rubber forming *Int. J. Preci. Engg. Manuf.* **15** 913–9
[18] Lekatou A, Sfikas A K, Petsa C and Karantzalis A E 2016 Al–Co alloys prepared by vacuum arc melting: correlating microstructure evolution and aqueous corrosion behavior with Co content *Metals* **6** 46
[19] Eskandari M J, Asadabad M A, Tafrishi R and Shafyei 2016 A evolution of nanostructure in Al 1050 sheet deformed by cryo-cross-rolling *J. Mat Engg Perform* **25** 1643–9
[20] Lee E K *et al* 2013 Enhanced corrosion resistance and fuel cell performance of Al1050 bipolar plate coated with TiN/Ti double layer *Energ Convers and Manag* **75** 727–33
[21] Lingappa M S, Srinath M S and Amarendra H J 2017 Microstructural and mechanical investigation of Aluminium alloy (Al 1050) melted by microwave hybrid heating *Mater. Res. Express* **4** 076504
[22] Kuo C W, Lin C M, Lai G H, Chen Y C, Chang Y T and Wu W 2007 Characterization and mechanism of 304 Stainless steel vibration welding *Mat Trans* **48** 2319–23
[23] Phadnis S V, Satpati A K, Muthe K P, Vyas J C and Sundaresan R I 2003 Comparison of rolled and heat treated SS304 in chloride solution using electrochemical and XPS techniques *Corr. Sci.* **45** 2467–83
[24] Seelam U M R and Suryanarayana C 2013 Metallography of sputter-deposited SS304+Al Coatings *Metallogr Microstruct Anal* **2** 287–98
[25] Maurya S D, Purushothaman M, Krishnan P S G and Nayak S K 2014 Effect of nano-calcium carbonate content on the properties of poly (urethane methacrylate) nanocomposites *J. Thermoplastic Compos Mat* **27** 1711–27
[26] Desai S, Suryawanshi M, Gaikwad M, Mane A, Kim J and Moholkar A 2017 Investigations on the thickness dependent structural, morphological, and optoelectronic properties of sprayed cadmium based transparent conducting oxide *Thin Solid Films* **628** 196–202
[27] Ye L, Meng X Y, Ji X, Li Z M and Tang J H 2009 Synthesis and characterization of expandable graphite–poly (methyl methacrylate) composite particles and their application to flame retardation of rigid polyurethane foams *Poly Degrad Stabil* **94** 971–9
[28] Ates M, Kamer L and Ozkan H 2015 Comparative analysis of poly (N-methylpyrrole) and its titanium dioxide nanocomposite film formations against equivalent electrical circuit model for the their corrosion-inhibition effects *High Perform. Poly.* **28** 75–84
[29] Oprea S, Vlad S and Aurelian S 2001 Poly(urethane-methacrylate)s. Synthesis and characterization *Polymer* **42** 7257–66
[30] Suresh R, Deepa M, Moganavally P and Sudha P N 2016 A study on biological and catalytic activity of CSB derivative and its Cobalt and Nickel complexes *Orient. J. Chem.* **32** 2509–16
[31] Khaparde A, Vijayalakshmi M A and Tetala K K R 2017 Development of a metal/chelate polyhydroxyethylmethacrylate monolith capillary for selective depletion of immunoglobulin G from human plasma for proteomics *J. Chromatography A* **1517** 117–25
[32] Naeimi H and Moradian M 2013 Encapsulation of copper (I)-Schiff base complex in NaYnanoporosity: an efficient and reusable catalyst in the synthesis of propargylamines via A3-coupling (aldehyde-amine-alkyne) reactions *App Cat A, General.* **467** 400–06

[33] Sun Y, Cao C, Huang P, Yang S and Song W 2015 Amines functionalized C60 as solid base catalysts for Knoevenagel condensation with high activity and stability *The Royal Soci Chem Adv.* **5** 86082–7

[34] Belage Y, Gawade N and Ningnure V 2016 Design and fabrication of test rig for measurement of thermal conductivity of composite slab *Int. J. Res. Eng. App. Manag.* **2** 26–9

[35] Sengottvel P and Jagadale K 2017 Thermal conductivity of composite slab *Int. J. Pure App. Math.* **116** 51–9